Int. J. Electrochem. Sci., 14 **(2019)** 7202 – 7212, doi: 10.20964/2019.08.19

International Journal of
ELECTROCHEMICAL
SCIENCE
www.electrochemsci.org

Short Communication

Effect of the Local Damage of a Sulfide Film Formed on Steel Surfaces in H_2S Environments

Wei Zhao[*]

College of mechanical and automotive engineering, Qilu University of Technology (Shandong Academy of Sciences), 250353 Jinan, China
[*]E-mail: zwapple@yeah.net

Received: 2 March 2019 / *Accepted:* 17 May 2019 / *Published:* 30 June 2019

The electrochemical corrosion behavior of X80 pipeline steel in distilled water with saturated H_2S at 323 K was evaluated, and the corrosion products were characterized. The results showed that mackinawite and cubic FeS were the primary and secondary crystalline phases observed, respectively. In addition, a series of changes in their size and shape occurred during the immersion processes. The sulfide film that formed on the steel surfaces enhanced the corrosion resistance. Moreover, zero resistance ammeter measurements showed that the galvanic effect was introduced between the fresh and sulfide film-covered steel electrodes, and then it decreased, and disappeared, indicating that substantial local corrosion cannot be introduced because of the local damage of the sulfide film.

Keywords: hydrogen sulfide corrosion; electrochemical corrosion; galvanic effect

1. INTRODUCTION

Hydrogen sulfide (H_2S) corrosion of pipeline steels has attracted attention because of the resulting metal dissolution, pitting corrosion, hydrogen embrittlement, hydrogen induced cracking and sulfide stress corrosion cracking [1-7]. In addition, this corrosion can decrease the cohesion of Fe-Fe atomic bonds and result in substantial reduction in the mechanical properties [8]. The sulfide film can be formed on the steel surface after immersion in a H_2S environment which has an important effect on further corrosion behaviors [9]. The sulfide film properties depend on the electrolyte, pH, temperature, H_2S partial pressure, and immersion time [10-17]. This film can act as an effective barrier against the diffusion of ions [18], inhibiting anodic dissolution [19, 20], although the film does not passivate the surface.

Local damage from the films formed by the corrosion products is inevitable for several reasons [5, 21, 22]. However, literature reports about the local damage of sulfide films and its effect on the

overall sulfide film properties and corrosion behavior are limited. In the present study, the characterization of corrosion products and their effect on the corrosion resistance were studied. In addition, the galvanic effect between the fresh steel electrodes and those covered with a film of the corrosion products was also studied by zero resistance ammeter (ZRA) measurements to evaluate the local damage from the sulfide film.

2. MATERIALS AND METHODS

2.1. Materials and samples

The steel used in this study was X80 pipeline steel in which the microstructure was polygonal ferrite and granular bainite. Its composition is shown in Table 1. The specimens, rectangular electrodes with a 1 cm^2 area, were ground using an 800 grit emery paper, and mounted in silica gel to prepare for the immersion and electrochemical tests.

Table 1. Composition of X80 pipeline steel used in this study (wt.%)

C	Si	Mn	Al	Nb	V	Ni	Cr	Mo	B	Ti	Ca	Cu	Fe
0.046	0.305	1.76	0.058	0.079	0.008	0.225	0.023	0.226	0.00025	0.015	0.001	0.215	Balanced

2.2. Immersion and electrochemical tests

The electrochemical tests were performed with a Gamry Interface 1000. A three-electrode cell was used in which a platinum plate was used as the counter electrode, and a saturated calomel electrode (SCE) of +0.241 V_{SHE} as the reference electrode. The solution used in this study was distilled water with saturated H_2S at 323 K (pH=4.21). Potentiodynamic polarization was conducted with a scanning rate of 0.5 mV/s. The galvanic current between two electrodes was measured using a zero resistance ammeter (ZRA) in which the distance between two electrodes was maintained at 5 cm. The area of fresh steel electrode without the corrosion product was maintained at 1 cm^2 and the area ratio between the two electrodes was changed by moving the steel electrode covered with the sulfide film.

2.3. Analyses of corrosion products

After immersion for 0.5, 4, 8, 16, 24 and 96 h, the corrosion products on the steel surface were characterized by scanning electron microscopy (SEM) on a JSM-6480LA instrument and X-ray diffraction (XRD) on a DX-2700 instrument with a scanning step of 0.5 °/min.

3. RESULTS AND DISCUSSION

3.1. Corrosion product characterization

As shown in Fig. 1, the corrosion products nucleated rapidly, and a series of changes in their size and shape can be observed. This observation is in accordance with previous studies [5, 19]. The

corrosion products were distributed uniformly with a beam-like shape and size on the nanoscale after immersion for 0.5 h. The shape changed to granular after immersion for 4 h, and they became more compact after immersion for 8 h. In addition, some defects were observed on the surface of the corrosion products, like holes, after immersion for 0.5 to 8 h. Long and narrow corrosion products with greater than 20 μm were formed after immersion for 16 h. The irregularly shaped corrosion products with obvious boundaries were present in which a mixture of holes could be seen after immersion for 24 h. It was suspected that the irregularly shaped corrosion products were formed by the growth of those with a long, narrow shape. The irregularly shaped corrosion products covered the entire surface after immersion for 96 h. The subtle difference in the corrosion product film characterization compared with previous studies can be attributed to the different environments, including the electrolyte, pH, temperature, H_2S partial pressure, and immersion time [10-17, 23].

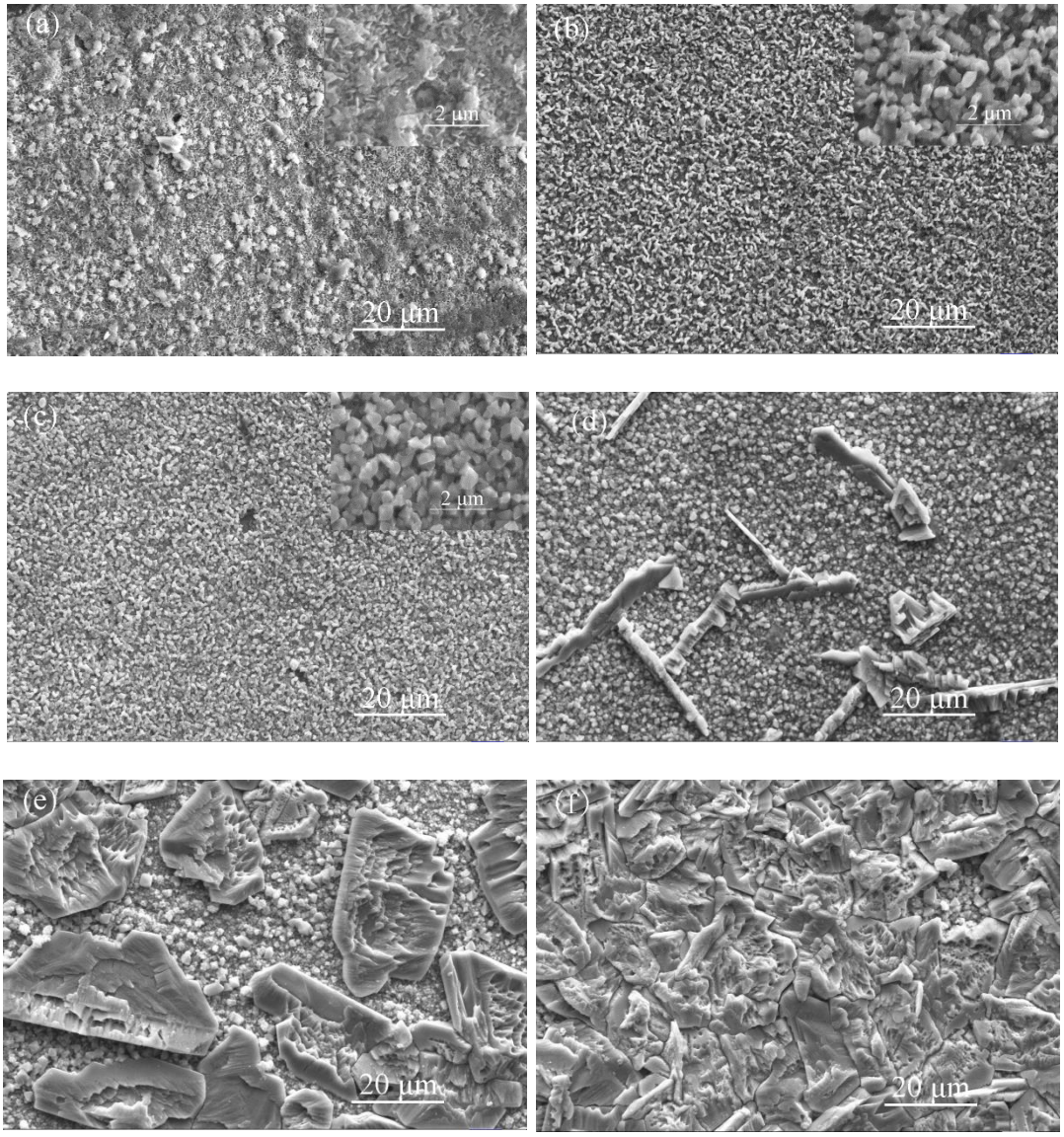

Figure 1. Micrographs of corrosion products formed on the steel surface in distilled water at 323 K with saturated H_2S after immersion for (a) 0.5, (b) 4, (c) 8, (d) 16, (e) 24, and (f) 96 h

As shown in Fig. 2, mackinawite was the initial corrosion product that was identified after 0.5 h. Cubic FeS was the secondary corrosion product that was identified after immersion for 16 h. Corresponding to the SEM micrographs, the beam-like and granular corrosion products with nanoscale sizes were mackinawite and the long, narrow shaped corrosion products were cubic FeS. Mackinawite and cubic FeS are two common corrosion products that form in H_2S environments. Mackinawite can transform to cubic FeS [5]. The mackinawite peaks appeared early compared to other electrolytes without Cl^- [5]. In addition, other crystal types were not detected, like pyrrhotite, troilite and pyrite, which can be attributed to the relatively low H_2S pressure. In the previous studies concerning H_2S corrosion in saline solution containing Cl^- in the similar temperature and H_2S partial pressure [5, 12], it was found that the corrosion products peaks were detected after immersion more than 16 h and the Fe peaks could not be detected after immersion for 96 h. It is indicated that the presence of Cl^- avoided the accumulation of the corrosion products on the steel surface in the initial immersion stages although it promoted the corrosion rate. However, the accumulation of corrosion products was promoted after it reached a critical value and the corrosion product films thickness increased much faster. The deeper mechanisms need a further study.

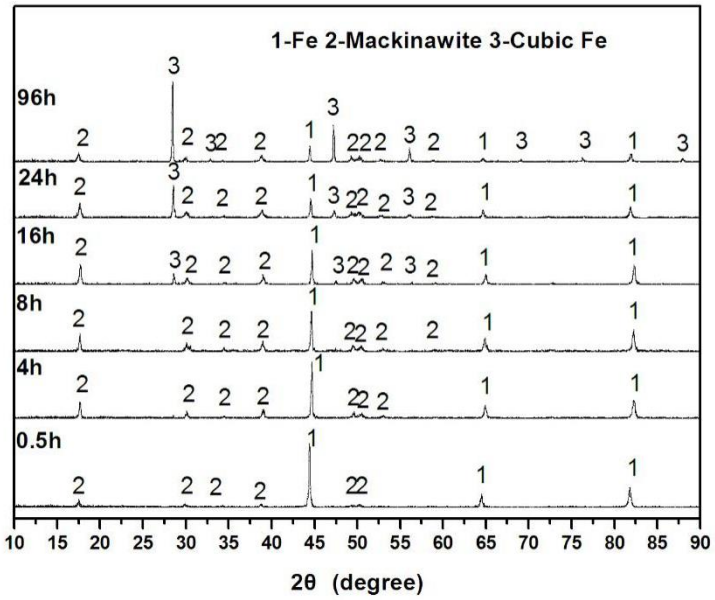

Figure 2. XRD patterns of corrosion product films in distilled water at 323 K with saturated H_2S after immersion for 0.5, 4, 8, 16, 24 and 96 h

3.2 Potentiodynamic polarization curves

The potentiodynamic polarization curves of X80 pipeline steel in distilled water after immersion for 0.5, 4, 8, 16, 24 and 96 h are shown in Fig. 3. In addition, the corrosion potential E_{corr}, corrosion current density i_{corr}, and cathodic and anodic Tafel slopes (β_a and β_c, respectively) from the extrapolation of the Tafel lines, are shown in Table 2. The E_{corr} increased obviously from -0.792 to -0.653 V vs.SCE which indicates that the corrosion driving force decreased as the immersion process continued. In addition, i_{corr} decreased from 84.38 to 0.25 $\mu A \cdot cm^{-2}$ indicating that the corrosion rate

decreased during the immersion processes, which can be attributed to the accumulation of the corrosion products and its density variation [24]. Previous studies have shown that the FeS particulates electrode has relatively high corrosion potential compared to the Fe electrode [25]. Thus, the increasing of the corrosion potential of the X80 pipeline steel can be attributed to accumulation of the corrosion products of FeS. In addition, compared with previous studies, the corrosion current density is lower than that of H_2S-saturated brine environments, which can be attributed to the formation of the different corrosion products [5, 12, 26, 27]. The distilled water with saturated H_2S was beneficial for the formation of fine crystals on a nano-scale, as is shown in Fig. 1.

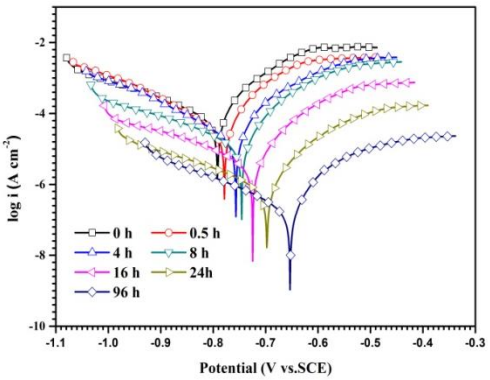

Figure 3. Potentiodynamic polarization curves of X80 steel in distilled water with saturated H_2S at 323 K after different immersion times of 0, 0.5, 4, 8, 16, 24 and 96 h

Table 2. Fitting results of potentiodynamic polarization curves by extrapolation of the Tafel lines

t(h)	E_{corr}(mV vs.SCE)	i_{corr}(μA cm^{-2})	β_a(mV dec^{-1})	β_c (mV dec^{-1})
0	-0.792	84.38	108	149
0.5	-0.779	35.43	142	139
4	-0.758	19.03	147	134
8	-0.746	17.80	148	225
16	-0.725	5.55	140	231
24	-0.698	0.99	143	218
96	-0.630	0.25	262	170

3.3 Electrochemical impedance spectroscopy

The EIS tests were conducted to evaluate the effects of corrosion product films on the corrosion behavior of X80 pipeline steel in distilled water with saturated H_2S at 323 K. The EIS results under

different immerion times are shown in Fig. 4. It is shown that all Nyquist plots only contained capacitive reactance loops and the magnitude of the capacitive loop represented by the semicircle diameter increased with immersion time. In addition, the peak of phase angle decreased and the corresponding frequency shifted to be lower as the immersion process developed, which is similar to previous studies [28].

Concerning some previous studies about H_2S corrosion [5, 6], the equivalent circuit of $R_s(C_{dl}R_{ct})$ and $R_s(Q_f(R_f(C_{dl}R_{ct})))$ were chosen to fit the EIS results after immersion for 0 h and other times, respectively. R_s, R_f and R_{ct} were the resistance of solution, corrosion product films and charge transfer resistance, respectively. Q_f was the constant-phase element (CPE) of sulfide corrosion product films, and C_{dl} is the double-layer capacitance. The fitted results are shown in Table 3. It was shown that the corrosion product films resistance R_f and charge transfer resistance R_{ct} increased as the immersion process developed indicating the corrosion resistance was enhanced.

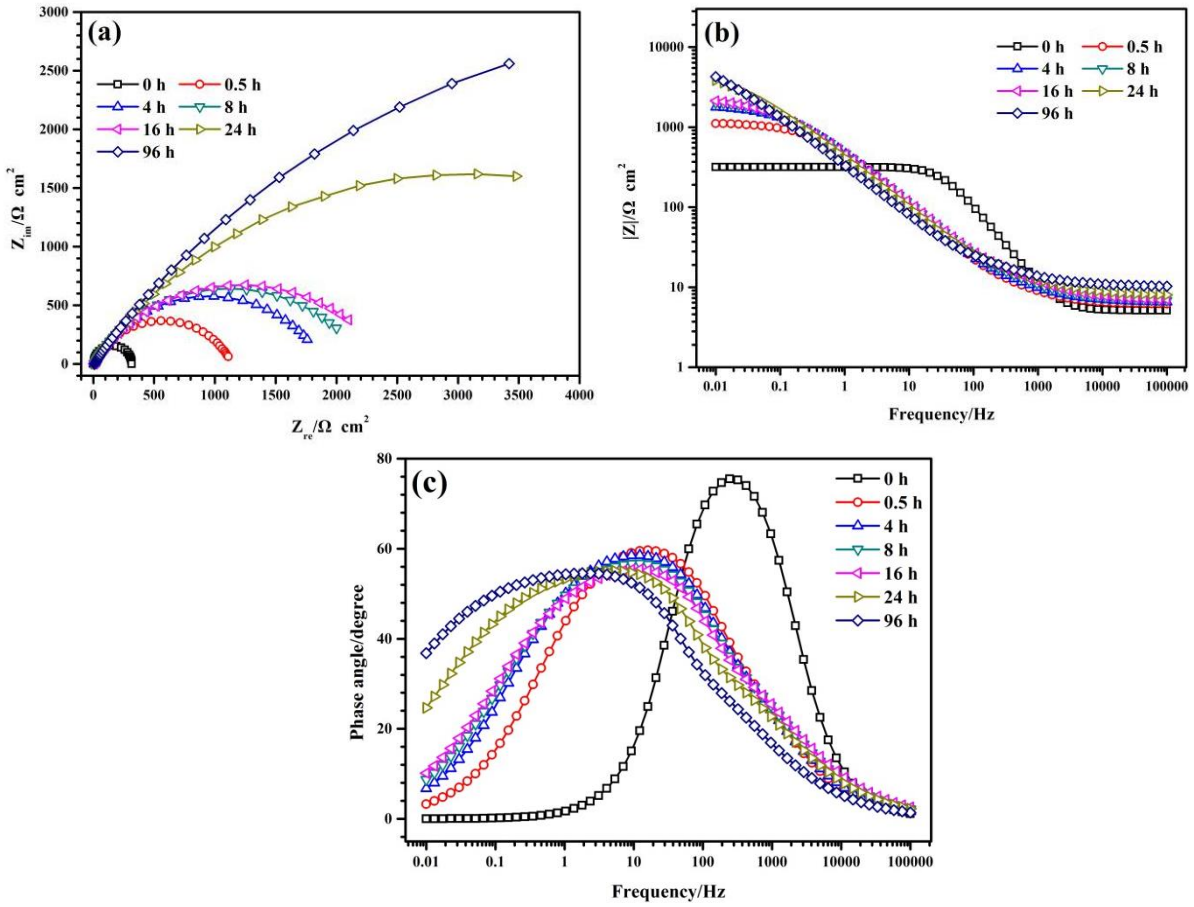

Figure 4. EIS results of X80 pipeline steel in distilled water with saturated H_2S at 323 K under different immerion times: (a) Nyquist plots; Bode plots of (b) impedance magnitude vs. frequency and (c) phase angle vs. Frequency

The potentiodynamic polarization curves and EIS results showed that the corrosion resistance increased as the immersion process developed which can be attributed to the effects of sulfide corrosion product films. In some previous studies [19], the corrosion resistance decreased in the initial

immersion process and then increased, and there was a inflection point which can be attributed to the porous, thin and chloride-riched corrosion products. However, the corrosion product film in the distilled water without chloride was compact and covered the whole steel surface, shown in Fig. 1. Thus, the corrosion resistance presented increase tendency in the immersion process.

Table 3. Fitted EIS values obtained under different immersion times

t(h)	R_s($\Omega\cdot cm^2$)	Q_f		R_f($\Omega\cdot cm^2$)	C_{dl}($\mu F\cdot cm^{-2}$)	R_{ct}($\Omega\cdot cm^2$)
		Y_0($\Omega^{-1}\cdot cm^{-2}\cdot S^n$)	n_{sl}			
0	5.12	--	--	--	15.12	312
0.5	6.09	0.0004127	0.6183	41.23	16.14	1098
2	6.32	0.0004832	0.6017	45.41	17.05	1234
4	6.41	0.0004958	0.5853	47.81	17.14	1854
8	6.65	0.0005324	0.5545	51.83	17.89	2189
16	6.81	0.0005654	0.5328	56.27	18.54	2385
24	7.78	0.0007154	0.5128	68.94	25.46	6083
48	8.95	0.0008032	0.5105	75.24	31.83	8054
96	10.12	0.0009189	0.5109	81.36	32.94	10981

3.3 Galvanic effect

A local damage of the sulfide film may occur because of some reasons, like flow velocity [22]. Thus, a galvanic current can be introduced because of the distinct corrosion potential between the steel electrodes with or without a coating of the corrosion product (Fig. 3b). Thus, the steel electrode without a coating of the corrosion product served as the anode and the electrode covered corrosion product served as the cathode when they are coupled because of the corrosion potential series. This is in accordance with previous studies [5].

The galvanic currents between the two electrodes are shown in Fig. 5. The galvanic current increased with the cathode/anode electrode area ratio and the immersion time of the electrodes that were covered with the corrosion product. More importantly, the current decreased and even disappeared as the processes continued.

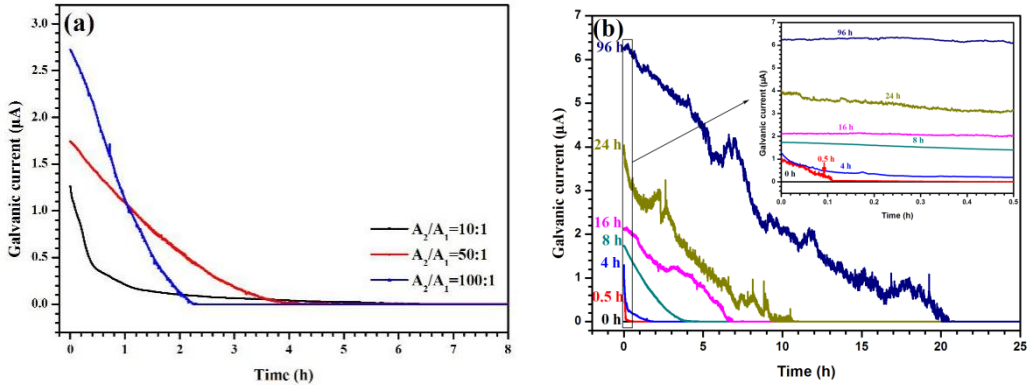

Figure 5. Galvanic current between steel electrodes with or without a coating of the corrosion product for (a) the same immersion time of the steel electrodes covered with the sulfide film (8h) and different cathode/anode electrode area ratios of 10:1, 50:1 and 100:1 and (b) the different immersion times of steel electrodes covered with the sulfide film (0, 0.5, 4, 8, 16, 24 and 96 h) and the same cathode/anode electrode area ratio of 50:1.

When the fresh steel electrode without a coating of the corrosion product films was immersed into the electrolyte alone, the following equations were used:

$$i_{a,\,fre} = i_{0,a1}\exp(\frac{E_{corr,\,fre} - E_{e,a}}{\beta_{a,\,fre}}) \tag{1}$$

$$\left|i_{c,\,fre}\right| = i_{0,c1}\exp(\frac{E_{e,c} - E_{corr,\,fre}}{\beta_{c,\,fre}}) \tag{2}$$

$$i_{a,\,fre} = \left|i_{c,\,fre}\right| = i_{corr,\,fre} \tag{3}$$

where $i_{a,fre}$ and $|i_{c,fre}|$ indicate the anodic dissolution and cathodic reduction current density, respectively; $i_{corr,fre}$ indicates the corrosion current density; $i_{0,a1}$ and $i_{0,c1}$ are the anode and cathode exchange current densities respectively; $E_{e,a}$ and $E_{e,c}$ are the anode and cathode reaction equilibrium electrode potentials, respectively; $\beta_{a,fre}$ and $\beta_{c,fre}$ are the anodic and cathodic Tafel slopes, respectively; and $E_{corr,fre}$ is the corrosion potential.

Combining Eq. (1) and (3), the following equation can be obtained:

$$\ln i_{corr,\,fre} = \frac{E_{e,c} - E_{e.a}}{\beta_{a,\,fre} + \beta_{c,\,fre}} + \frac{\beta_{a,\,fre}}{\beta_{a,\,fre} + \beta_{c,\,fre}}\ln i_{0,a1} + \frac{\beta_{c,\,fre}}{\beta_{a,\,fre} + \beta_{c,\,fre}}\ln i_{0,c1} \tag{4}$$

When the two electrodes were coupled, they can be regarded as an iso-potential plane because of the good conductivity of the material [29]. Thus, the galvanic current I_g can be expressed as follows:

$$I_g = i_g A_{fre} = i_{a,g} A_{fre} - \left|i_{c1,g}\right| A_{fre} = \left|i_{c2,g}\right| A_{cov} \tag{5}$$

where i_g is the galvanic current density for the fresh steel electrode that is not covered with corrosion products; A_{fre} and A_{cov} are the areas of the electrodes without and with a coating of the corrosion product, respectively; $i_{a,g}$ is the anodic dissolution current density; and $i_{c1,g}$ and $i_{c2,g}$ are the cathodic current densities for the electrodes without and with a coating of the corrosion product, respectively.

The value of $i_{a,g}$ can be calculated as follows:

$$i_{a,g} = i_{0,a1}\exp(\frac{E_g - E_{e.a}}{\beta_{a,\,fre}}) \tag{6}$$

or $$i_{a,g} = i_{corr,fre} \exp(\frac{E_g - E_{corr,fre}}{\beta_{a,fre}}) \quad (7)$$

where E_g is the galvanic potential.

The value of $|i_{c1,g}|$ can be calculated as follows:

$$\left|i_{c1,g}\right| = i_{0,c1} \exp(\frac{E_{e,c} - E_g}{\beta_{c,fre}}) \quad (8)$$

or $$\left|i_{c1,g}\right| = i_{corr,fre} \exp(\frac{E_{corr,fre} - E_g}{\beta_{c,fre}}) \quad (9)$$

The value of $|i_{c2,g}|$ can be calculated as follows:

$$\left|i_{c2,g}\right| = i_{0,c2} \exp(\frac{E_{e,c} - E_g}{\beta_{c,cov}}) \quad (10)$$

or $$\left|i_{c2,g}\right| = i_{corr,cov} \exp(\frac{E_{corr,cov} - E_g}{\beta_{c,cov}}) \quad (11)$$

where $i_{0,c2}$, $E_{corr,cov}$ and $i_{corr,cov}$ are the cathodic reaction exchange current density, corrosion potential and corrosion current density for the electrode covered with the corrosion product, respectively.

The galvanic corrosion factor γ is expressed as the promotion of the galvanic effect on the anodic dissolution of the fresh steel electrode, as follows:

$$\gamma = \frac{i_{a,g}}{i_{corr,fre}} \quad (12)$$

The galvanic corrosion factor γ is difficult to calculate by Eqs. (4)-(12) without simplification because of the complexity of the equations. Thus, it is necessary to make simplifications. When the immersion time of the sulfide film-covered electrode is relatively short (e.g., 0.5 h), the surface conditions of the two electrodes can be viewed as the same indicating that their cathode Tafel slopes can be viewed as the same. Thus, the Napierian logarithm of γ can be expressed as follows:

$$\ln\gamma = \ln(\frac{i_{a,g}}{i_{corr,fre}}) = \frac{\beta_{c,fre}}{\beta_{a,fre} + \beta_{c,fre}} \ln(1 + \frac{A_{cov}}{A_{fre}} \times \frac{i_{0,c2}}{i_{0,c1}}) \quad (13)$$

When the immersion time of the electrode that was covered with the corrosion product was relatively long, a substantial anodic polarization occurred on the fresh steel electrode surface, indicating that I_{c1} can be neglected [21, 30, 31]. Thus, the Napierian logarithm of γ can be calculated as follows:

$$\ln\gamma = \ln(\frac{I_{a,g}}{I_{corr,fre}}) = \frac{E_{corr,cov} - E_{corr,fre}}{\beta_{c,cov} + \beta_{a,fre}} + \frac{\beta_{c,cov}}{\beta_{c,cov} + \beta_{a,fre}} \ln(\frac{A_{cov}}{A_{fre}} \times \frac{I_{corr,cov}}{I_{corr,fre}}) \quad (14)$$

It can be seen from Eqs. (13) and (14) that the galvanic corrosion factor γ was positive relative to the area ratio of A_{cov}/A_{fre} which explains the results shown in Fig. 4a. In addition, γ was positive relative to the distinct corrosion potential $E_{corr,cov}$-$E_{corr,fre}$ and the ratio of corrosion current density $I_{corr,cov}/I_{corr,fre}$ explains the results shown in Fig. 4b.

In addition, the galvanic current rapidly decreased, even disappeared. This indicates that the surface condition of the fresh steel electrode changed and became similar to that of the steel electrode covered with the corrosion product. Compared with the formation of the galvanic current, anions of S^{2-} and HS^- migrated to the anode due to the electric field. The precipitation of the corrosion products

occurred and a new corrosion product film was formed because of the reactions between the accumulated S^{2-}, HS^- and Fe^{2+}.

It is indicated that the sulfide corrosion product films are stable and unacted on the local damage. However, the conclusion can't be analogized to other corrosion environments. It was found that a serious localized corrosion may be introduced due to the local damage of the corrosion products in CO_2 environments. However, the similar results were also found in NACE A solution in previous studies [5], indicating that this phenomenon was indenpendent on the chloridion. However, the effects of temperature and H_2S partial pressure need further studies.

4. CONCLUSIONS

1. Mackinawite and cubic FeS were the initial and secondary crystalline corrosion products, respectively. In addition, a series of changes in the shape, size and composition of corrosion products were observed.

2. The potentiodynamic polarization results showed that the corrosion resistance improved with the development of the immersion process and the increase in the amount of corrosion products.

3. A galvanic current was generated between the two electrodes with and without a coating of the corrosion products. However, the current decreased and then disappeared because of the formation of the new corrosion product film.

ACKNOWLEDGEMENTS
The work was supported by the National Nature Science Foundation of China (No. 51805285), the National Nature Science Foundation of China (No. 51605237), the Natural Science Foundation of Shandong Province of China (ZR2017LEE011) and the Key Research and Development Project of Shandong Province (2018GGX103031).

References

1. M. Al-Mansour, A.M. Alfantazi, and M. EI-boujdaini, *Mater. Design*, 30 (2009) 4088.
2. C. Zhou, S. Zheng, C. Chen, and G. Lu, *Corros. Sci.*, 67 (2013) 184.
3. Q. Sha, and D. Li, *Mat. Sci. Eng. A*, 585 (2013) 214.
4. C. Yu, X. Gao, and H. Wang, *Mate.r Lett.*, 209(2017) 459.
5. W. Zhao, Y. Zou, K. Matsuda and Z.D. Zou, *Corros. Sci.*, 102(2016) 455.
6. W. Zhao, Y. Zou, K. Matsuda, and Z.D. Zou, *Mater. Design.*, 99(2016) 44.
7. K. Chong, H. Zhang, G.C. Xiao, and W. Zhao, *Int. J. Electrochem. Sci.*, 13(2018) 6858.
8. P. Wang, Z. Lv, S. Zheng, Y. Qi, J. Wang, and Y. Zheng, *Int. J. Hydrogen Energy*, 40 (2015) 1.
9. X.L Wen, P.P Bai, B.W. Luo, S.Q. Z, and C.F. Chen, *Corros. Sci.*, 139(2018) 124.
10. P.P. Bai, S.Q. Zheng, H. Zhao, Y. Ding, J. Wu, and C.F. Chen, *Corros. Sci.*, 87 (2014) 397.
11. S.Q. Zheng, C. Zhou, X. Chen, L. Zhang, J. Zheng, and Y. Zhao, *Int. J. Hydrogen Energy*, 39 (2014) 13919.
12. P.P Bai, H. Zhao, S.Q. Zheng, and C. Chen, *Corros. Sci.*, 93 (2015) 109.
13. P.C. Okonkwo, M.H. Sliem, R.A. Shakoor, A.M.A. Mohamed, and A.M. Abdullah, *J. Mater. Eng. Perform*, 26(2017):3775-83.
14. F.X. Shi, L. Zhang, J.W. Yang, M.X. Lua, J.H. Ding, and H. Lia, *Corros. Sci.*, 102(2016) 103.

15. W.M. Song, G.R. Yang, B.B. Liao, J. Li, Y. Ma, and Y. Hao, *J. Wuhan Univ. Technol.*, 33(2018)1205.
16. F. Pessu, Y. Hua, R. Barker, and A. Neville, *Corrosion*, 74(2018) 886.
17. Z. Wang, M. Liu, M. Lu, L. Zhang, J. Sun, Z. Zhang, X. Tang, *Int. J. Electrochem. Sci.*, 13(2018) 915.
18. M. Liu, J. Wang, W. Ke, E.H. Han, *J. Mater. Sci. Technol*., 30 (2014) 504.
19. P.P. Bai, S.Q. Zheng, and C. Chen, *Mater. Chem. Phys.*, 149–150 (2015) 295.
20. M.N. Zafar, and R. Rihan, *Corros. Sci.*, 94 (2015) 275.
21. G.A. Zhang, N. Yu, L.Y. Yang, and X.P. Guo, *Corros. Sci.*, 86 (2014) 202.
22. L.W. Wang, Z.Y. Liu, Z.Y. Cui, C.W. Du, X.H. Wang, and X.G. Li, *Corros. Sci.*, 85 (2014) 401.
23. N.Y. Zhang, D.Z. Zeng, Z. Zhang, W.T. Zhao, and G.J. Yao, *Corros. Eng. Sci. Techn.*, 53 (2018) 370.
24. Q. Liu, Z. Li, Z.Y. Liu, X.G. Li, and S.Q. Wang, *J. Mater. Eng. Perform*, 26 (2017) 2763.
25. Z. Liu, X. Gao, L. Du, J. Li, P. Li, X. Bai, and R.D.K. Misra, *J. Mater. Eng. Perform*, 26 (2017) 1010.
26. P.P. Bai, Y.X. Liang, S.Q. Zheng, and C.F. Chen, *Ind. Eng. Chem. Res.*, 55 (2016) 10932.
27. F. Huang, P. Cheng, Y.Y. Dong, J. Liu, Q. Hu, X.Y. Zhao, and Y.F. Cheng, *J. Mater. Eng. Perform*, 26 (2017) 828.
28. Z. Liu, X. Gao, L. Du, J. Li, P. Li, C. Yu, R.D.K. Misr, and Y. Wang, *Electrochim. Acta*, 232 (2017) 528.
29. F.M. AlAbbas, C. Williamson, S.M. Bhola, J.R. Spear, D.L. Olson, B. Mishra, and A.E. Kakpovbia, *Int. Biodeter. Biodegr*., 78 (2013) 34.
30. L.W. Wang, Z.Y. Liu, Z.Y. Cui, C.W. Du, X.H. Wang, and X.G. Li, *Corros. Sci.*, 85 (2014) 401.
31. G.A. Zhang, and Y.F. Cheng, *Electrochim. Acta*, 56 (2011) 1676.
32. G.A. Zhang, and Y.F. Cheng, *Corros. Sci.*, 52 (2010) 960.